PNAS NEXUS

PNAS Nexus, 2025, 4, pgaf151
https://doi.org/10.1093/pnasnexus/pgaf151
Advance access publication 10 May 2025
Research Report

PROTON ATPASE TRANSLOCATION CONTROL 1-mediated H$^+$-ATPase translocation boosts plant growth under drought by optimizing root and leaf functions

Naoya Katsuhama[a], Kazuma Sakoda[a], Haruki Kimura[b], Yutaro Shimizu[b,c], Yuuki Sakai[d], Kenji Nagata[e], Mitsutomo Abe[e], Ichiro Terashima[a,f] and Wataru Yamori[a,*]

[a]Department of Agricultural and Environmental Biology, Graduate School of Agricultural and Life Sciences, The University of Tokyo, Tokyo 113-8657, Japan
[b]Department of Biological Sciences, Graduate School of Science, The University of Tokyo, Tokyo 113-0033, Japan
[c]Center for Sustainable Resource Science, RIKEN, Wako 351-0198, Japan
[d]Graduate School of Science, Kobe University, Kobe 657-8501, Japan
[e]Department of Life Sciences, Graduate School of Arts and Sciences, The University of Tokyo, Tokyo 153-8902, Japan
[f]Institute of Molecular Biology, National Chung Hsing University, Taichung 40227, Taiwan
*To whom correspondence should be addressed: Email: yamori@g.ecc.u-tokyo.ac.jp
Edited By Ivet Bahar

Abstract

Optimizing leaf photosynthesis and root water and mineral uptake in crops during drought is crucial for enhancing agricultural productivity under climate change. Although plasma membrane H$^+$-ATPase plays a key role in plant physiological processes, its overexpression alone does not consistently improve growth. While PROTON ATPASE TRANSLOCATION CONTROL 1 (PATROL1) regulates H$^+$-ATPase translocation in response to various environmental stimuli in leaves, its function in roots remains largely unknown. Here, we show that H$^+$-ATPase was coimmunoprecipitated with PATROL1 in roots of *Arabidopsis thaliana*. Under hyperosmotic stress, *PATROL1* overexpression line had significantly greater root length and lateral root numbers than wild type (WT) and knockout lines. Micrografting between WT and *PATROL1* knockout or overexpression lines showed that PATROL1 is indispensable in both shoots and roots, indicating that root uptake and leaf photosynthesis are simultaneous limiting factors for plant growth under soil water deficit. Compared with the WT, *PATROL1* overexpression in whole plants resulted in a 41% increase in shoot dry weight and a 43% increase in shoot nitrogen content under drought conditions. These findings highlight the potential of H$^+$-ATPase regulation in both roots and shoots as a new strategy to improve plant productivity, particularly under drought conditions.

Keywords: *Arabidopsis thaliana*, H$^+$-ATPase, root, photosynthesis, drought

Significance Statement

The plasma membrane H$^+$-ATPase is essential for stomatal opening in response to light, with its translocation in guard cells regulated by PROTON ATPASE TRANSLOCATION CONTROL 1 (PATROL1), the plant ortholog of the mammalian membrane trafficking factor Munc13. While H$^+$-ATPase also supports nutrient uptake and stress responses in roots, the role of root PATROL1 has remained elusive. We found that PATROL1 interacts with H$^+$-ATPase in roots as well as shoots, alters its localization under hyperosmotic stress, and controls root length and number. PATROL1 influences the growth of both shoots and roots, with its overexpression enhancing nitrogen assimilation and photosynthesis under drought conditions. This study highlights that synergistically enhancing root function and photosynthesis through *PATROL1* overexpression could be a feasible strategy for developing drought-tolerant crops.

Introduction

Drought presents a major challenge to agricultural production, especially in meeting the food demands of the world's growing population under climate change (1). Yield reduction due to drought occurs when the water uptake, which is essential for nutrients supply and photosynthetic assimilation, is restricted (2, 3). Drought tolerance can take various forms; however, from an agricultural perspective, optimizing water use and capture within the limitation of available soil moisture during gradual and moderate soil water deficits is the most effective adaptation (4, 5). In this scenario, robust leaf growth and photosynthesis, supported by efficient water and nutrient uptake through enhanced root system architecture and activity, are key traits to minimizing yield penalties or failure (2, 3). In addition, coregulating photosynthesis and nutrient uptake is advocated as a breeding strategy for improving yield and resource use

Competing Interest: The authors declare no competing interests.
Received: January 18, 2025. **Accepted:** May 2, 2025

efficiency even under sufficient irrigation (6–8). However, maintaining an excessive root system and its functions consume carbon and energy (4, 9). Therefore, uncovering root phenotypic plasticity in response to fluctuating soil moisture and nutrient conditions is essential for designing an ideal root system (10, 11).

Since plasma membrane (PM) H^+-ATPase plays key roles in plant growth, such as hypocotyl and root elongation, mineral nutrient acquisition, stomatal opening, and environmental stress responses (12), modulating PM H^+-ATPase is a potential strategy to improve root uptake and photosynthesis under drought and resource scarcity (13). For instance, overexpression of *Arabidopsis thaliana* H^+-ATPase 2 (AHA2) in the guard cell promoted light-induced stomatal opening and enhanced growth in *A. thaliana* (14) and a *Populus* sp. hybrid (15). Moreover, overexpression of *Oryza sativa* H^+-ATPase 1 in whole plants increased grain yield by simultaneously improving nutrient uptake, photosynthesis, sugar translocation, and nutrient enrichment (7). On the contrary, excessive or constitutive PM H^+-ATPase activity can have adverse effects, including growth impairment, male sterility, necrotic lesions, and severe dehydration, because PM H^+-ATPase is an ATP-consuming protein with numerous physiological roles (16, 17). Therefore, both the quantity and timing of PM H^+-ATPase activity should be precisely regulated to develop drought-tolerant plants while managing associated trade-offs.

Most previous studies of PM H^+-ATPase regulation focused on transcriptional and post-translational modifications, particularly the phosphorylation and dephosphorylation of autoinhibitory C-terminal residues (12, 13). PROTON ATPASE TRANSLOCATION CONTROL 1 (PATROL1) was discovered as a unique regulatory factor for *A. thaliana* H^+-ATPase 1 (AHA1) (18). PATROL1 is a plant ortholog of mammalian uncoordinated 13s (Munc13s), and it contains a MUN domain (Fig. S1) which is responsible for synaptic vesicle priming in neuronal exocytosis in animals (18, 19). PATROL1 rapidly tethers an appropriate amount of AHA1 to the PM of stomatal guard cells in response to changes in light, CO_2 concentration ($[CO_2]$), abscisic acid, osmotic pressure, and leaf detachment (20). Systemic overexpression of *PATROL1* (*PATROL1*-OX) enhances photosynthesis and biomass production under fluctuating light conditions, while maintaining water use efficiency by ensuring rapid stomatal movement (21). A recent study using a *patrol1* loss-of-function mutant showed that PATROL1 is also involved in primary root elongation by regulating the root meristematic size (22). In addition, shoot growth of wild-type (WT) plants was reduced when shoot was grafted onto *patrol1* rootstock (22). Although PATROL1 is expressed in both shoots and roots (18, 22), its specific function in roots and their contributions to shoot growth under drought remain unknown.

Here, we examined the distribution pattern and interaction of PATROL1 with AHAs in the roots of *A. thaliana*. We then analyzed the expression and intracellular dynamics of PATROL1 and the root system architecture in WT, *PATROL1* knockout, and overexpression lines under PEG-simulated drought conditions. Finally, we investigated the distinct roles of PATROL1 in roots and shoots, focusing on nitrogen uptake and photosynthesis under moderate drought stress, aiming at developing a novel strategy for enhancing crop drought tolerance by regulating PM H^+-ATPase activity.

Results

PATROL1 distribution pattern and coimmunoprecipitation with PM H^+-ATPase in roots

PATROL1-OX promotes photosynthesis induction and growth under fluctuating light conditions owing to rapid stomatal movement (21). To investigate other functions of PATROL1, we grew *A. thaliana* WT, *PATROL1* knockout (*patrol1*), and *PATROL1*-OX plants under elevated $[CO_2]$, at which stomatal conductance does not limit photosynthesis. Shoot growth of *patrol1* was significantly reduced by 28% relative to WT and by 32% relative to *PATROL1*-OX (Fig. 1A). Although the photosynthetic property of *patrol1* increased as $[CO_2]$ elevated, it remained significantly lower than that of WT and *PATROL1*-OX (Fig. S2A and B). These results suggest that stomatal limitation is not the sole cause of the impaired CO_2 assimilation and growth in *patrol1* (Figs. 1A and S2C).

We further explored PATROL1 functions besides stomatal regulation. We examined the expression pattern of *PATROL1* in β-glucuronidase (GUS) reporter lines. In these plants, PATROL1 fused to GUS at the N terminus (GUS-PATROL1) was expressed under the control of the *PATROL1* regulatory sequence. GUS activity was ubiquitous in *gPATROL1:GUS-PATROL1; patrol1* (*gPATROL1:GUS-PATROL1*) seedlings, with higher levels in the vascular bundles, meristematic regions of shoot and primary root, and lateral root primordia (Figs. 1B and S3A). In the root elongation and maturation zones, it was moderate in epidermis, cortex, and pericycle (Fig. 1B). We also investigated the subcellular localization of the PATROL1 protein, expressed under the control of the *PATROL1* regulatory sequences, by observing enhanced green fluorescent protein (EGFP)-tagged PATROL1 in *gPATROL1:EGFP-PATROL1; patrol1* (*gPATROL1:EGFP-PATROL1*) plants. The expression pattern of EGFP-PATROL1 in roots was very similar to that of GUS-PATROL1, and EGFP fluorescence was detected in almost all cells, including root epidermal cells, in which EGFP-PATROL1 appeared in the cytosol along the PM (Fig. 1C).

In stomatal guard cells and subsidiary cells, PATROL1 plays key roles in regulating the trafficking of AHAs to and from the PM (18, 23). However, it is unclear whether it also interacts with AHAs in the root. To better understand the relationship between PATROL1 and AHAs in underground parts, we performed coimmunoprecipitation (co-IP) experiments using protein extracts from roots of GFP-PATROL1 or GFP plants. Co-IP of substantial AHA2 (and possible other AHAs: Table S2) with GFP-PATROL1, but virtually none with the free GFP control (Fig. 1D), suggests that PATROL1 interacts with AHAs in root cells. Taken together, our results support a model in which plant growth could be affected by the interaction of PATROL1 and PM H^+-ATPase in roots.

PATROL1 is essential for root elongation and branching under PEG-simulated drought

To test our hypothesis on the role of PATROL1 in optimizing root growth under soil moisture deficit, we examined how transgenic *A. thaliana* roots respond under hyperosmotic stress. Seedlings were grown on 1/2 Murashige and Skoog (MS) medium for 5 days and then transferred to 1/2 MS medium treated with or without 30% (w/v) PEG 6000 for another 10 days. In PEG medium, *PATROL1*-OX plants relatively sustained roots and shoots growth, but that of WT and *patrol1* plants was inhibited (Fig. 2A right). In the control medium, growth of *PATROL1*-OX was comparable to that of WT, but that of *patrol1* was somewhat smaller (Fig. 2A left). The components of the root system and the relative growth of PEG treatment compared with the mean of control were analyzed to assess the impact on root growth. In the control medium, root length and number of WT and *PATROL1*-OX were statistically equivalent, but those of *patrol1* were significantly less (Fig. 2E–G left). Under hyperosmotic stress, they were significantly greater in *PATROL1*-OX than in WT and significantly less in *patrol1* (Fig. 2E–G right). The primary root length of WT decreased by 12% of the control (Fig. 2E), lateral root length by 54% (Fig. 2F), and lateral root number by 31% (Fig. 2G). Interestingly, those of *patrol1* and

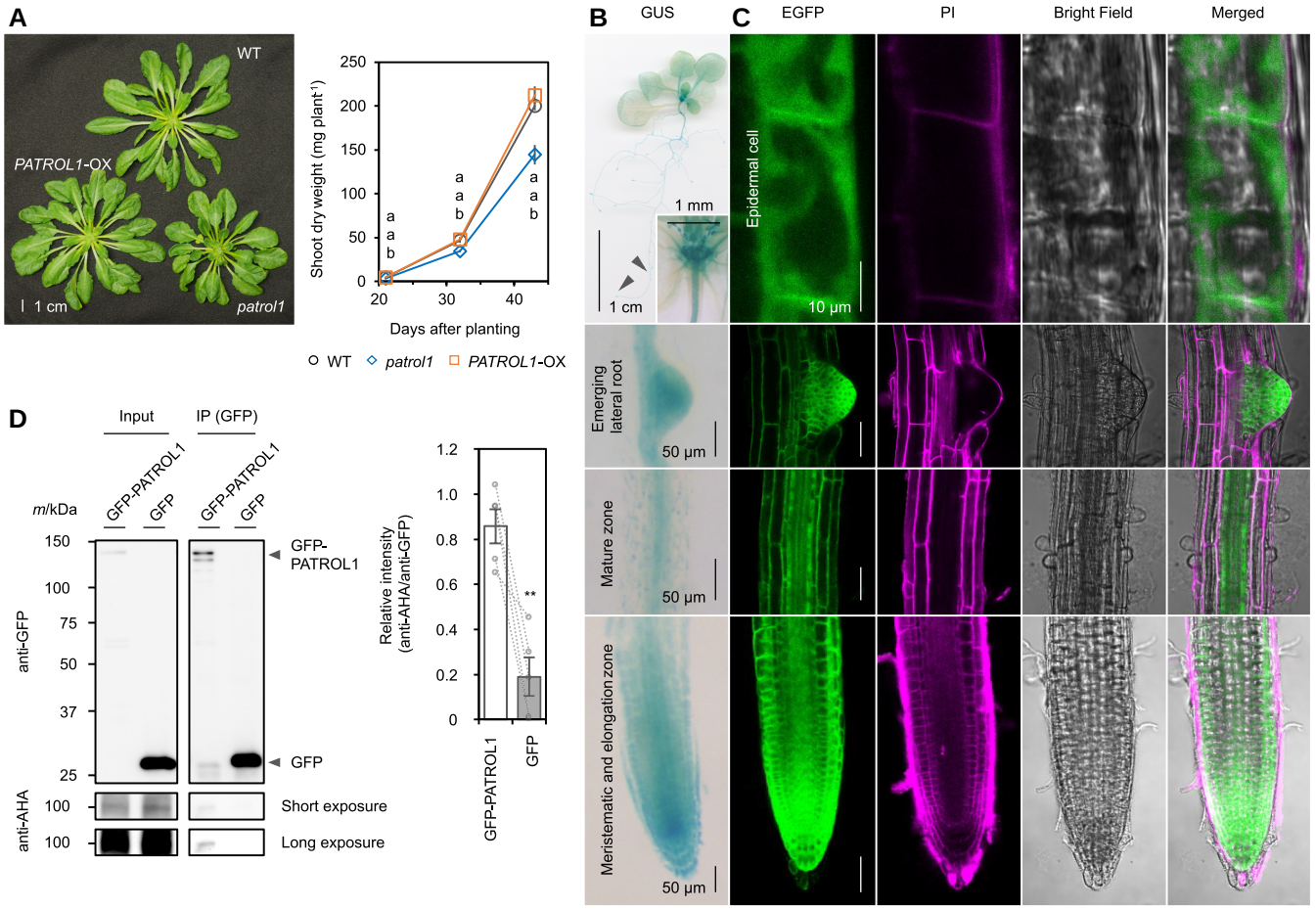

Fig. 1. Localization of PATROL1 and interaction with AHAs in the roots of *A. thaliana*. A) Phenotype and shoot dry weight of WT, *patrol1*, and *PATROL1*-OX plants grown at elevated [CO_2] (1,500 μmol mol^{-1}) with steady light (PPFD of 100 μmol m^{-2} s^{-1}) for 43 days. Error bars represent SEM ($n = 7$). Means not sharing any letters are significantly different between genotypes at $P < 0.05$ by Tukey–Kramer test. B) GUS staining of 2-week-old *gPATROL1:GUS-PATROL1* plants. C) Subcellular localization of EGFP-PATROL1 in 2-week-old *A. thaliana* primary root. Green, EGFP-PATROL1 localization; magenta cell wall propidium iodide (PI) staining. D) Association of GFP-PATROL1 and AHAs observed by co-IP assay in the root. Total proteins (input) from the transgenic *A. thaliana* roots producing either GFP-PATROL1 or GFP alone (negative control) were immunoprecipitated with anti-GFP beads. The inputs and immunoprecipitates were immunoblotted with anti-AHA and anti-GFP antibodies. Error bars represent SEM ($n = 5$). ** indicates statistically significant differences by Student's t test at $P < 0.01$.

PATROL1-OX decreased by 4 and 4%, 30 and 32%, and 14 and 6%, respectively, of WT (Fig. 2E–G). Chlorophyll fluorescence imaging confirmed that hyperosmotic treatment reduced the quantum yield of PSII (Y(II)) and increased nonphotochemical quenching (NPQ) of *patrol1*, while all three lines showed similar trends in the control (Fig. 2A and B). Overall, *PATROL1*-OX had 53% greater shoot fresh weight and 37% greater root fresh weight than WT, while *patrol1* had 33 and 41%, respectively, less (Fig. 2C and D).

We next sought to determine how hyperosmotic stress affects the expression and intracellular dynamics of *PATROL1* in roots. qRT-PCR analysis revealed that *PATROL1* expression was slightly up-regulated in roots after exposure to PEG (Fig. 3A). Moreover, 30-min exposure to osmotic stress increased EGFP-PATROL1 dots (18) in the peripheral cytoplasm of root epidermal cells within the elongation zone of transgenic plants expressing EGFP-PATROL1 driven by its native promoter (Figs. 3C and S4). GFP-PATROL1 dots colocalize with AHA1 in guard cells and subsidiary cells (18, 22). Also, these dots are sensitive to inhibitors of phosphoinositide 4-kinase (PI4 K), a signaling component of PMs, in both leaf and root cells, indicating that PATROL1 dots mediate the translocation of target proteins through a PI4K-dependent mechanism (22, 23). This increase in EGFP-PATROL1 dots suggests that the localization of PATROL1 in roots is regulated in response to hyperosmotic stress, as well as transcriptionally. Proteins with a MUN domain in plants are classified under the Domain of Unknown Function 810 (DUF810). Notably, the expression levels of five other DUF810 and AHA member genes were consistent across WT, *patrol1*, and *PATROL1*-OX plants under control condition (Fig. S5).

PATROL1-OX enhances root water and nitrogen uptake and improves photosynthesis under moderate drought conditions

To assess the contribution of PATROL1 to plant growth under soil water deficit, we grew WT, *patrol1*, and *PATROL1*-OX plants together in a single pot for 16 days with sufficient water and then withheld watering for 21 days (Fig. 4A). While the soil volumetric water content (VWC) of the control ranged between 0.50 and 0.61 m^3 m^{-3}, those of the treatment pots gradually decreased from 0.60 to 0.07 m^3 m^{-3} due to evapotranspiration (Fig. 4B). Under drought, the shoot dry weight and projected leaf area of *PATROL1*-OX were 41 and 34%, respectively, higher than WT, and those of *patrol1* were 31 and 18%, respectively, lower than WT (Fig. 4C and D right). In the control, there were no significant

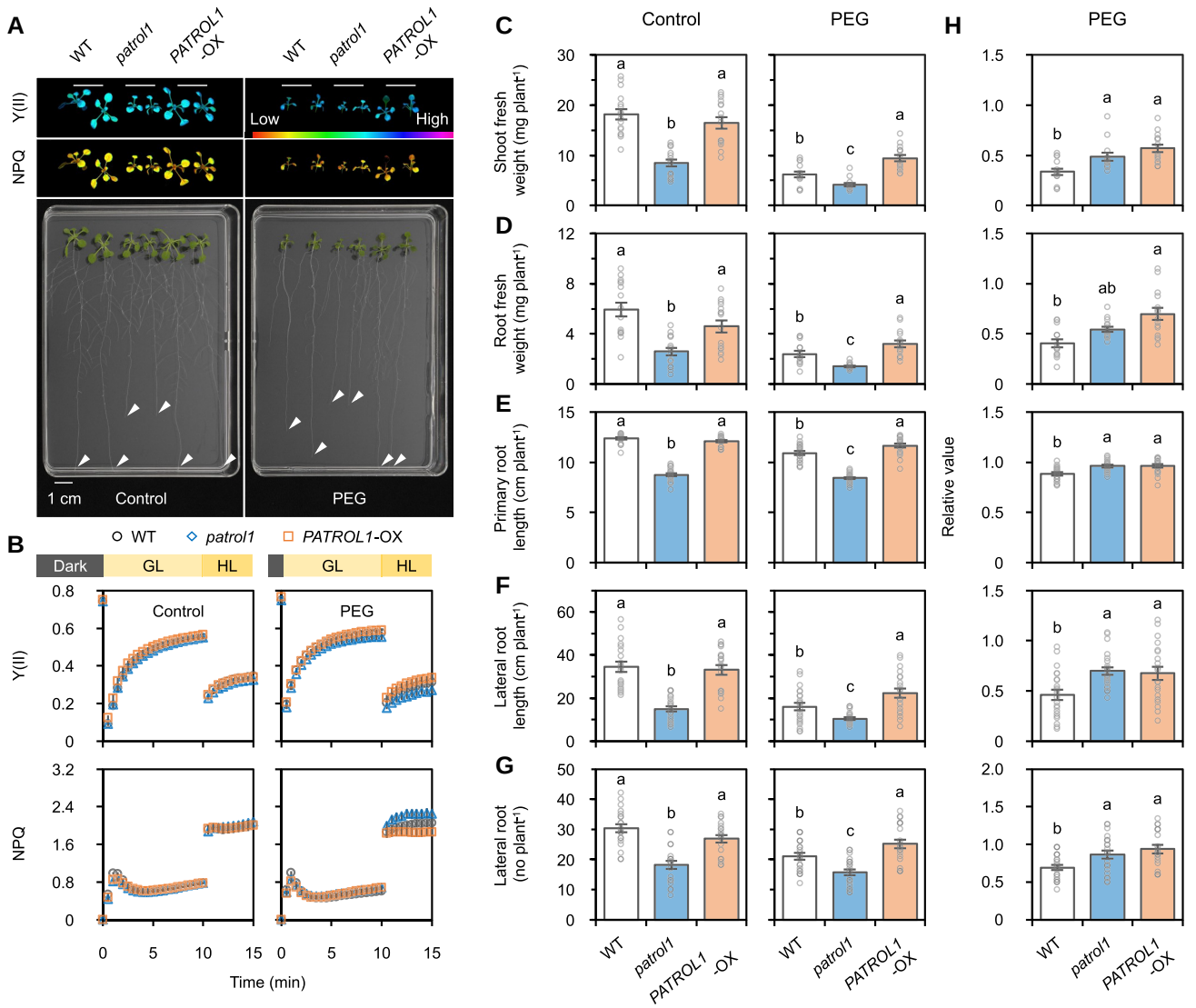

Fig. 2. Shoot and root growth of *PATROL1* transgenic plants under PEG-simulated drought conditions. A) Phenotype of WT, *patrol1*, and *PATROL1*-OX plants grown on 1/2 MS medium treated with or without 30% (w/v) PEG 6000 for 10 days. Scale bar, 1 cm. B) Postillumination induction of the quantum yield of PSII (Y(II)) and NPQ, measured under GL (PPFD of 100 µmol m^{-2} s^{-1}) and HL (PPFD of 500 µmol m^{-2} s^{-1}) after overnight dark adaptation. Error bars represent SEM ($n = 8$–12). C) Shoot fresh weight; D) root fresh weights; E) primary root length; F) lateral root length; G) lateral root numbers of treated and untreated plants. H) Values in PEG treatment relative to the average control values were calculated as an indicator of stress tolerance. Error bars represent SEM ($n = 20$–22). Means not sharing any letters are significantly different between genotypes at $P < 0.05$ by Tukey–Kramer test.

differences in either among the genotypes (Fig. 4C and D left). In the control, carbon isotope ($\delta^{13}C$) discrimination, which reflects stomatal closure and CO_2 diffusion during growth, was identical among genotypes, but under drought, it increased significantly in *patrol1* above WT (Fig. 4E).

To gain a deeper understanding of the photosynthetic response to soil dehydration, we obtained spatial and time-resolved chlorophyll fluorescence parameters of plants grown at photosynthetically active photon flux density (PPFD) of 100 µmol m^{-2} s^{-1} (Fig. 4L). The maximum quantum yield of PSII (F_v/F_m) and steady-state Y(II) of the treated plants decreased as the drought progressed, especially in *patrol1* (Fig. 4F and G). Concurrently, NPQ of *patrol1* decreased significantly after 3 weeks of drought treatment (Fig. 4H), while the quantum yield of regulated thermal dissipation in PSII (Y(NPQ)) remained comparable among genotypes (Fig. 4I). This reduction in NPQ suggests that the energy dissipation mechanism in *patrol1* was severely impaired under prolonged stress (24). As Y(NPQ) remained stable in *patrol1* plants while Y(II) decreased, excess excitation energy was unrelatedly dissipated as the quantum yield of nonregulated energy dissipation in PSII (Y(NO)) (Fig. 4J), which may have led to the formation of reactive oxygen species (25, 26). Together, $\delta^{13}C$ and chlorophyll fluorescence measurements indicate that electron-sink limitation of photosynthesis, induced by stomatal closure from restricted water uptake in the rhizosphere, may have caused photoinhibition in *patrol1*, which was more pronounced under higher irradiance (Fig. S6).

Finally, to clarify the independent contributions of shoot and root PATROL1 to drought tolerance, we micrografted *A. thaliana* scions and rootstocks with different PATROL1 expression levels (Fig. 5A). Soil VWC in the control ranged between 0.43 and 0.58 m^3 m^{-3}, but under drought it decreased from 0.59 to 0.04 m^3 m^{-3} after 24 days. Under drought conditions, plants with *patrol1* as either scion or rootstock (i.e. KO scion/KO rootstock, KO/WT, and WT/KO plants) had significantly lower shoot dry weight (Fig. 5B), significantly less C content (Fig. 5D), and smaller leaf area (Fig. 5C) and shoot N content (Fig. 5E) than

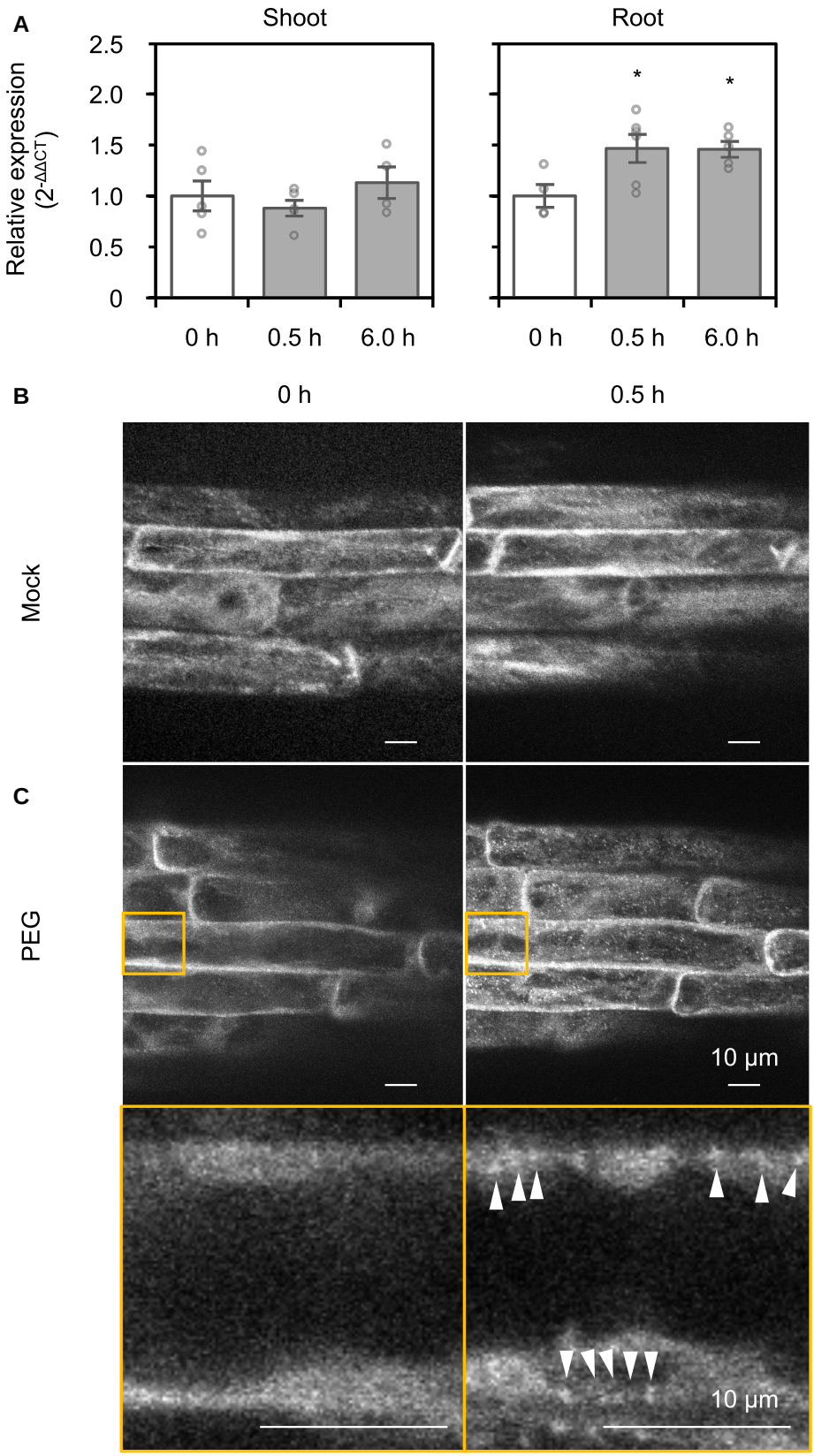

Fig. 3. Regulation of root *PATROL1* transcripts and protein localization in response to PEG-induced hyperosmotic stress. A) qRT-PCR analysis of *PATROL1* in shoot and root. Nineteen-day-old *A. thaliana* were treated with 30% (w/v) PEG 6000 for designed times. The expression level of *PATROL1* at 0.0 h of treatment was normalized as 1.0. Error bars represent SEM ($n = 4$–5). * Significant differences between means at $P < 0.05$ by Dunnett's test. Representative image of root epidermal cells from 1-week-old *gPATROL1:EGFP-PATROL1* transgenic plants treated with liquid 1/2 MS medium ($n = 4$) (B) or liquid 1/2 MS medium with 10% (w/v) PEG 8000 ($n = 7$) (C) for 0.5 h. Arrowheads indicate EGFP-PATROL1 dots in endosomes responding to osmotic stress. Maximum projection images were generated from five serial Z-slices with a 1-μm interval before and after mock or PEG treatment. Enlarged images of the areas enclosed by yellow squares were taken from a single slice. Scale bar, 10 μm.

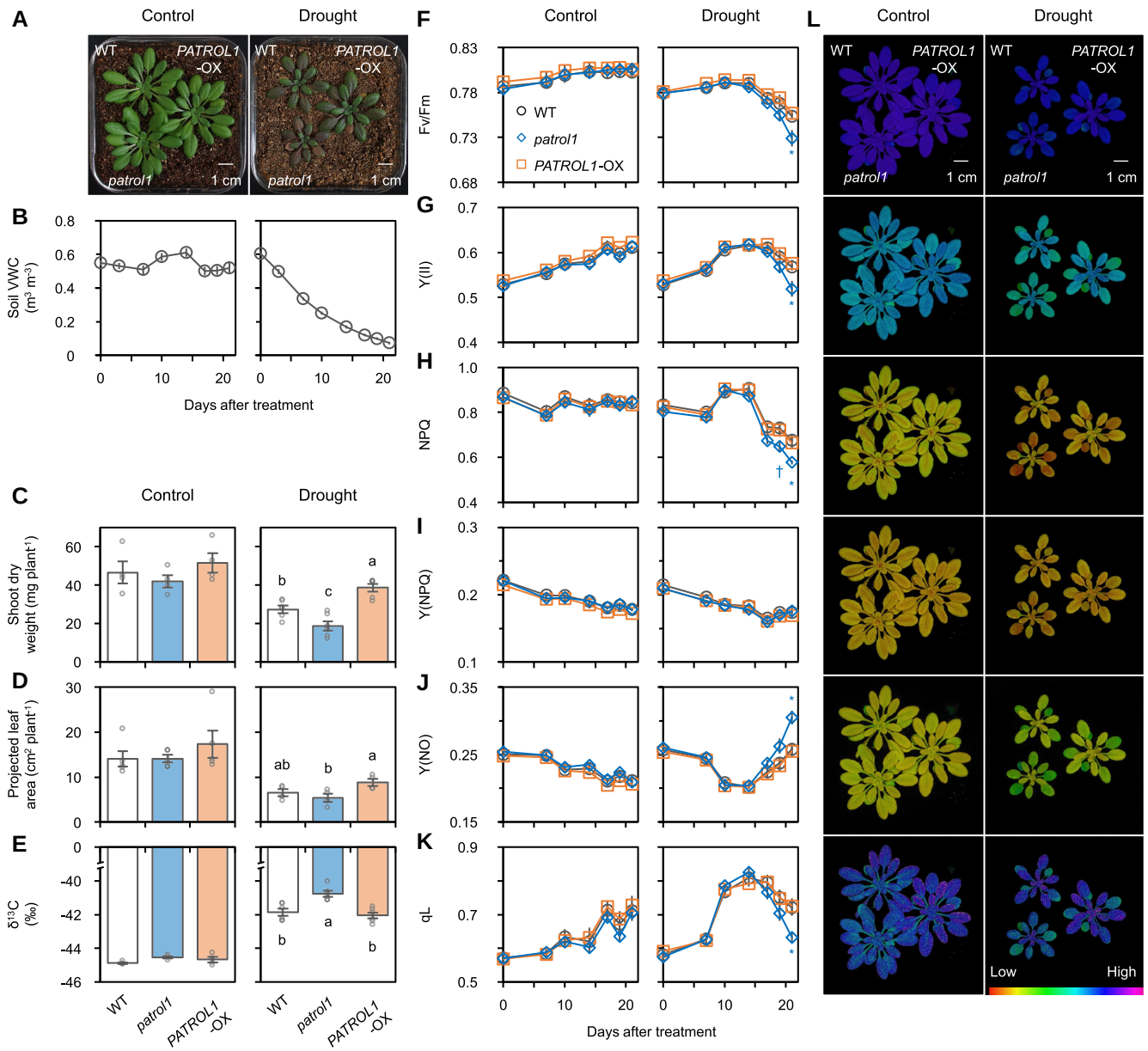

Fig. 4. Photochemical activities and growth of *PATROL1* transgenic plants under drought conditions. A) Phenotype of WT, *patrol1*, and *PATROL1*-OX plants after withholding water for 21 days. B) Soil VWC; C) shoot dry weight; D) projected leaf area; E) $\delta^{13}C$ discrimination of harvested shoots. Error bars represent SEM ($n = 4$–6). Means not sharing any letters are significantly different between genotypes at $P < 0.05$ by Tukey–Kramer test. F) Maximum quantum yield of PSII (F_v/F_m) after overnight dark adaptation. G) Steady-state quantum yield of PSII (Y(II)); H) NPQ; I) quantum yield of regulated thermal dissipation in PSII (Y(NPQ)); J) that of nonregulated energy dissipation in PSII (Y(NO)); K) the fraction of open PSII reaction centers (qL) were measured under PPFD of 100 μmol m^{-2} s^{-1}. Error bars represent SEM ($n = 4$–5). Significant differences between WT and transgenic plants at $^*P < 0.05$ and †0.10 by Dunnett's test. L) Visualization of steady-state photochemical activities under PPFD of 100 μmol m^{-2} s^{-1}. Scale bar, 1 cm.

WT/WT plants. On the contrary, plants with *PATROL1*-OX as either scion or rootstock (i.e. OX/OX, OX/WT, and WT/OX plants) had a greater value than WT/WT plants (Fig. 5B–E). Consequently, there were strong positive correlations between shoot dry weight, C content, and N content in all genotypes under drought (Fig. 6). In addition, the trend of Y(II) was comparable to shoot growth, being higher in grafted plants including *PATROL1*-OX and lower in plants including *patrol1* (Fig. S7B). Under drought, NPQ was lowest in KO/WT, followed by WT/WT, KO/KO, and WT/KO (Fig. S7C). Also, the lowest NPQ was observed in WT/OX, followed by OX/OX, OX/WT, and WT/WT. The leaf chlorophyll content (SPAD) value was significantly higher in OX/OX than in WT/WT and lower in WT/KO (Fig. S7A). Under control conditions, there were no differences in plant growth or photosynthesis among genotypes (Figs. 5 and S7). In summary, the importance of PATROL1 is comparable between shoots and roots, suggesting that both root uptake and leaf photosynthesis limit plant growth under drought conditions.

Discussion

Enhancing photosynthesis and improving root water and nutrient uptake are essential for achieving drought tolerance and adaptation under anticipated climate change (2). Plants may encounter spatial and temporal variations in solar radiation and

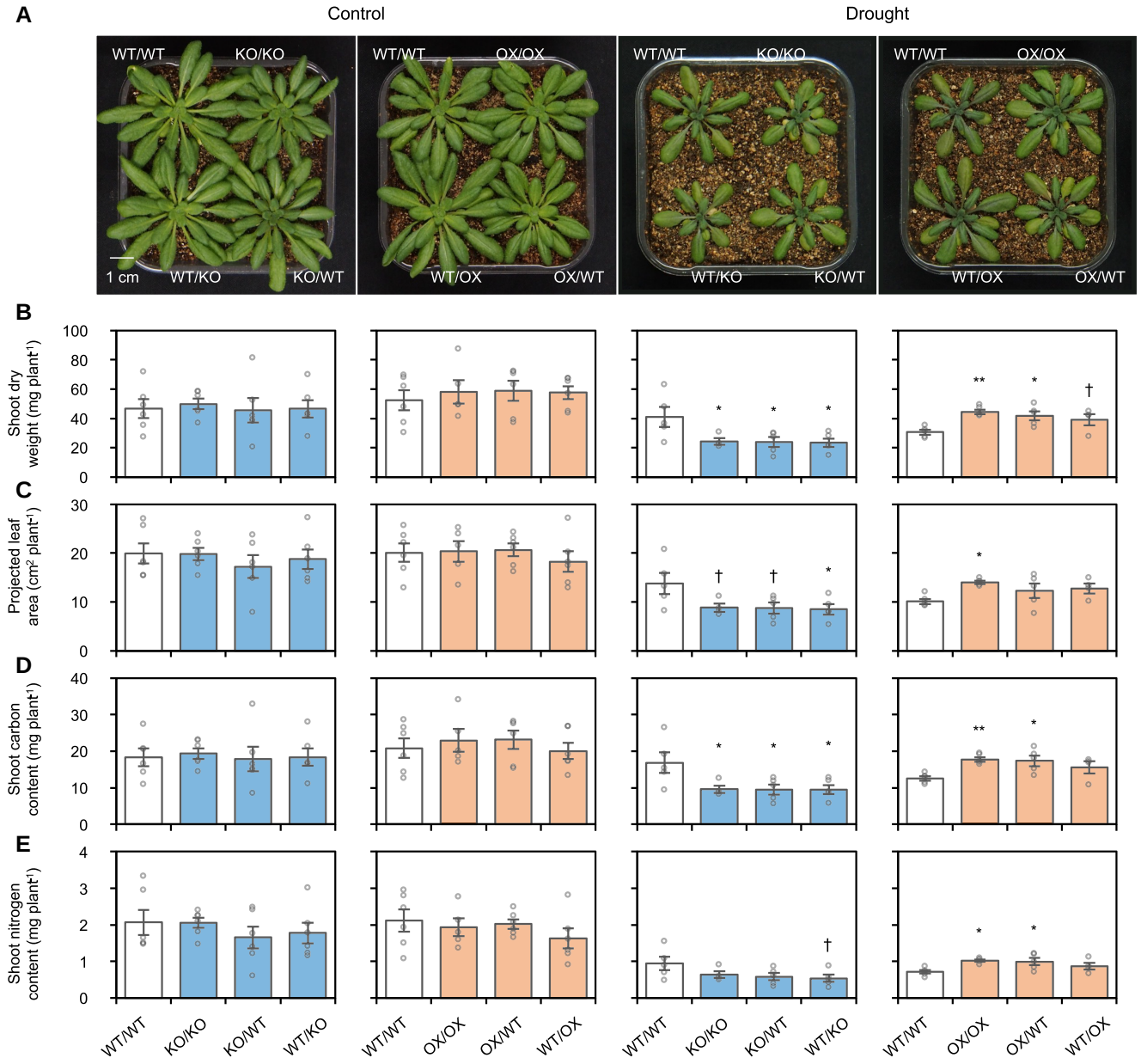

Fig. 5. Drought tolerance in grafted plants with different *PATROL1* expression levels in scion and rootstock. A) Growth performance; B) shoot dry weight; C) projected leaf area; D), E) shoot C and N contents of grafted plants after withholding water for 24 days. Error bars represent SEM ($n = 4$–6). Significant differences between WT/WT (scion/rootstock) and transgenic grafted plants at *$P < 0.01$, **0.05, and †0.10 by Dunnett's test. Scale bar, 1 cm.

atmospheric conditions (4), soil moisture, and nutrient availability (11). Therefore, it is vital for field-grown crops to have highly plastic root and shoot phenotypes to cope with these challenges (27). We showed that *PATROL1*-OX enhances photosynthesis and biomass production through vigorous root growth and increased N uptake under water deficit (Figs. 2 and 4–6). We also showed that PATROL1 in roots interacts with AHAs and alters its localization under hyperosmotic stress (Figs. 1 and 3). These results indicate that PATROL1 regulates PM H^+-ATPase localization in response to changing environment (e.g. water and nutrients availability), not only in leaves (18, 23, 28) but also in roots. We previously demonstrated that rapid stomatal movement of *PATROL1*-OX plants improved photosynthesis and biomass gain under fluctuating light and adequate irrigation (21). Thus, optimizing PM H^+-ATPase trafficking in both shoots and roots by modulating the single gene *PATROL1* could serve as an adaptive strategy to improve plant growth in both optimal and sub-optimal environments.

The present GUS reporter assay and qRT-PCR analysis confirmed that *PATROL1* is ubiquitously expressed throughout the plant (Figs. 1B and S5), which corroborates with previous studies (18, 22). The confocal microscopic analysis confirmed that the PATROL1 level is notably high in the meristematic regions of shoots and primary roots, lateral root primordia, and root stelae (Fig. 1C), where it plays a key role in root growth and water and nutrient foraging (11). In addition, as the maximum CO_2 assimilation rate and Y(II) of *patrol1* plants remained suppressed even under high [CO_2] (Fig. S2B) with steady light, indicating that reduced stomatal conductance is not the sole cause of the growth reduction (Fig. 1A). Overall, these results raise the question of how

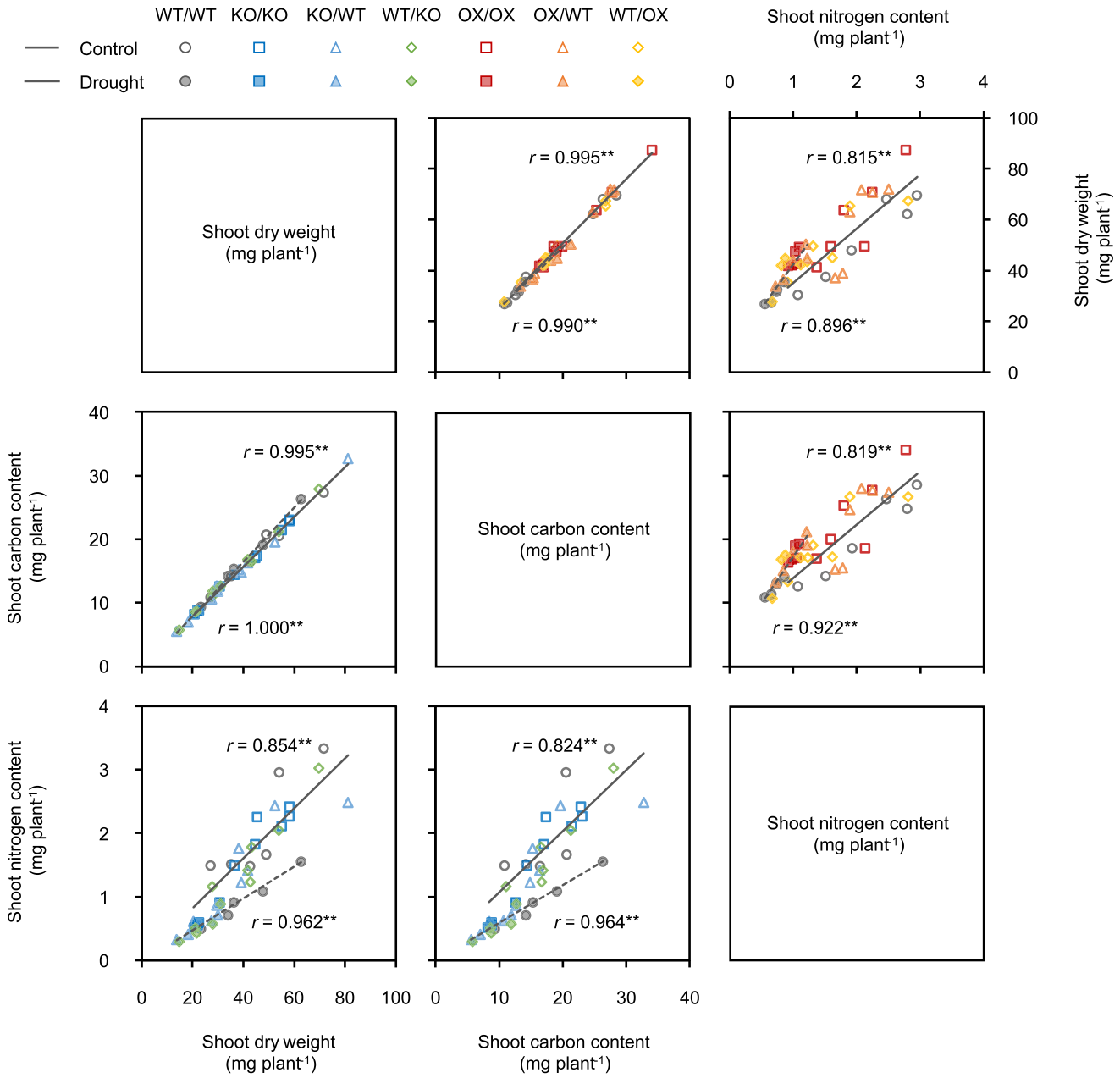

Fig. 6. Correlation matrix of shoot dry weight, C content, and N content under drought conditions. ** Significant Pearson's correlation at $P < 0.01$ ($n = 19$–24).

PATROL1 in both shoots and roots contributes to plant growth. Micrografting between WT and *patrol1* or *PATROL1*-OX plants revealed that PATROL1 is indispensable in both shoots and roots, indicating that root uptake and leaf photosynthesis are simultaneous limiting factors for plant growth under drought conditions (Fig. 5). Grafted plants with higher transpiration demand than their root water supply (WT/KO, OX/WT) had greater NPQ and less linear electron flow activity than combinations with the converse (KO/WT, WT/OX) under drought (Fig. S7B and C). This indicates that effective root water and nutrient foraging are essential for preventing dehydration and maintaining photosynthesis during soil drying. However, the reduced shoot growth in KO/WT plants and the lack of growth enhancement in WT/OX relative to WT/WT suggest that carbon gain from photosynthesis limited the root improvement (Fig. 5B–E), as root growth also depends on sufficient C allocation (4). Overall, *PATROL1* overexpression in both roots and shoots (OX/OX) enhanced shoot growth, N and C assimilation, and chlorophyll content (Figs. 5B–E and S7A), emphasizing the need for simultaneous enhancement of root functions and leaf photosynthesis to improve biomass production under drought. In other words, plant growth under drought stress may be constrained by the shortest supply of either water and nutrient uptake from roots or carbon gain from leaves, akin to the concept of Liebig's law of the minimum. Ultimately, *PATROL1* overexpression throughout the plant enhanced drought tolerance, resulting in increased photosynthesis and shoot biomass relative to WT under moderate drought conditions (Fig. 4).

Co-IP of AHAs with PATROL1 (Fig. 1D) suggests a direct or indirect interaction between them in roots. PATROL1 may contribute to drought tolerance by facilitating membrane trafficking,

particularly the delivery of PM H^+-ATPase (18). PATROL1 is related to mammalian uncoordinated 13s (Munc13s), which are involved in tethering, docking, and rapid fusion of transport vesicles and target membranes through interactions with SNAREs (soluble N-ethylmaleimide-sensitive factor attachment protein receptors) (29). PATROL1 contains a MUN domain (Fig. S1), a critical region also found in Munc13-1 (30, 31). Recent studies have revealed that SNAREs also interact with AHAs (32–36), and potentially with PATROL1, as indicated by immunoprecipitation mass spectrometric analysis (37). In this context, PATROL1 could ensure proper trafficking of PM H^+-ATPase either via SNAREs or directly. Moreover, the altered localization of PATROL1-GFP dots in the root epidermal cells in response to PEG treatment (Fig. 3C) is consistent with previous studies (18, 22, 23, 28), as well as transcriptional regulation (Fig. 3A). Together with the co-IP result (Fig. 1D), these results support the hypothesis that PATROL1 in roots colocalizes with and possibly regulates PM H^+-ATPase activity in response to hyperosmotic stress.

There is a growing recognition of the roles of PM H^+-ATPase in root system plasticity and nutrient uptake under various conditions (12). Here, we show that under PEG-induced water deficit, *PATROL1*-OX plants had significantly greater total root length and lateral root numbers (Fig. 2E–G) than WT and *patrol1* plants. Furthermore, N accumulation tended to decrease in *patrol1* and increase in *PATROL1*-OX plants under drought (Fig. 5E), resulting in significant strong positive correlations between shoot N, C, and growth (Fig. 6). Although we did not confirm the colocalization of AHAs, the distribution patterns of PATROL1 in the primary root tip, mature zone, and lateral root tip (Figs. 1C and S3B) closely resemble those of AHA1, AHA2, and AHA7 (38–41). It was reported that greater H^+ secretion by PM H^+-ATPase in the root tip sustains root elongation and root hair growth under moderate water stress in both *A. thaliana* and *O. sativa* (42). A recent study using bromocresol purple assessment showed that *patrol1* roots released less H^+ than WT roots, while *PATROL1*-OX roots released more (22). However, the similarity of expression patterns of *AHA* family members in WT, *patrol1*, and *PATROL1*-OX across all lines (Fig. S5) suggests that PATROL1 regulates PM H^+-ATPase activity posttranscriptionally rather than transcriptionally. Down-regulation of AHA1, AHA2, and AHA7 leads to auxin hypersensitivity and inhibits root elongation, while constitutive AHA1 activation has the opposite effect (43). Live imaging shows AHA2 localized at the root surface, with stronger signals at the root tip, and its accumulation in the cytoplasm reduces H^+ secretion when root elongation is suppressed (38). AHA2 also promotes root branching and growth in response to N availability (39, 44) and enhances hydrotropism under hyperosmotic stress (45, 46). Constitutive AHA1 activation enhances root elongation, increases shoot mineral contents (e.g. N, K, Ca, S, P), and boosts shoot biomass under nutrient-deficient conditions (47). Similarly, overexpression of *O. sativa* H^+-ATPase 1 in rice enhances root nutrient uptake and transportation, increasing leaf N, K, P, and Ca (48). Recent research also indicates that PM H^+-ATPase activity contributes to nitrate assimilation in *A. thaliana* leaves (49). Collectively, these findings suggest that PM H^+-ATPase plays a crucial role in nutrient uptake and transport by proton motive force (13). The consistency of enhanced root growth, increased shoot N content, and improved drought tolerance in *PATROL1*-OX plants with known functions of PM H^+-ATPase indicates that PATROL1 promotes root plasticity and activity under soil water stress by regulating PM H^+-ATPase activity. In addition, since cellulose synthase complexes are another identified cargo of PATROL1-mediated PM trafficking (50) and sustained cellulose synthesis are important under salt and hyperosmotic stress (51), root elongation and drought tolerance could also be linked to cellulose biosynthesis.

In conclusion, we have uncovered a new function of the membrane trafficking factor PATROL1 in root system plasticity, N uptake, and biomass production in response to water deficit. As PATROL1 is conserved among higher plants (18), our findings suggest that enhancing PM H^+-ATPase regulation through PATROL1 overexpression could be a promising strategy for developing drought-tolerant crops. Further research on the interactions between PATROL1, PM H^+-ATPase, and candidate proteins such as SNAREs will be crucial to elucidating the mechanisms underlying these phenotypes.

Methods

Plant materials and growth conditions

We used *A. thaliana* WT (Col-0), a *patrol1* knockout mutant, and *p35S:GFP-PATROL1; patrol1* overexpression lines (*PATROL1*-OX) (18). We generated *gPATROL1:GUS-PATROL1; patrol1* (*gPATROL1:GUS-PATROL1*) and *gPATROL1:EGFP-PATROL1; patrol1* (*gPATROL1:EGFP-PATROL1*) transgenic lines. Sterilized seeds were planted in 380-mL pots filled with a mixture of equal volumes of vermiculite and nutrient soil (Metromix 350; Sun Gro Horticulture, USA). The plants were grown in a growth chamber (NK System, Japan) at 23 °C with a relative humidity of 65%, a PPFD of 100 µmol m^{-2} s^{-1}, and an atmospheric [CO_2] of 400 µmol mol^{-1} under a 10-h light period. For elevated [CO_2] experiment, plants were grown at a [CO_2] of 1,500 µmol mol^{-1} under an 8-h light period.

Drought stress was induced by withholding water for 21 days from 16-day-old intact plants grown in soil and for 24 days from 27-day-old grafted plants. Soil VWC was determined every 2 to 4 ds by the gravimetric method, where:

$$\text{VWC } (m^3\ m^{-3}) = \frac{\text{Wet soil weight (kg)} - \text{dry soil weight (kg)}}{\text{Pot volume } (m^3)}.$$

For hyperosmotic stress treatment, 5-day-old seedlings were transferred to vertically oriented solid medium (1/2 MS, 1% sucrose, 0.05% 2-(*N*-morpholino)ethanesulfonic acid (MES), pH 5.7, 0.8% gellan gum), which was first dehydrated with 30% (w/v) PEG 6000 (FUJIFILM Wako Pure Chemical, Japan), and grown for an additional 10 days.

Micrografting

Transgenic plants were micrografted as described (52, 53), with modifications. In brief, seeds were surface-sterilized, soaked in distilled water, and kept in the dark at 4 °C for 3 days to synchronize germination. They were sown on a square petri dish containing 1% agar medium (1/2 MS, 1% sucrose, 0.05% MES, pH 5.7) and grown vertically in the dark at 23 °C for 2 days. The petri dishes were then moved to a 10-h light period with a PPFD of 100 µmol m^{-2} s^{-1} for 2 days. Next, hypocotyls were cut with a disposable razor blade (FA-10; FEATHER Safety Razor, Japan) and 90°-butt-grafted (52) on a nylon membrane (RPN119B; GE Healthcare, USA) placed on top of 2% agar medium (1/2 MS, 1% sucrose, 0.05% MES, pH 5.7). The grafted plants were incubated at a 45° angle under a PPFD of 50 µmol m^{-2} s^{-1} for 2 days and then 100 µmol m^{-2} s^{-1} for 4 days. Adventitious roots from the scion were removed, and the grafted plants were transferred to 1% agar medium (without nylon membrane) for an additional 5 days. Finally, adventitious roots were removed again before the grafted plants were transplanted into pots filled with soil.

Plasmid construction

To prepare the construct comprising PATROL1 fused to GUS or EGFP at the N terminus (GUS-PATROL1 or EGFP-PATROL1) under the control of the *PATROL1* regulatory sequence, we amplified the 5′-upstream region of *PATROL1* and the coding sequence of *GUS* or *EGFP* by PCR using appropriate templates and cloned together into the PstI/EcoRI-digested pRI201AN vector (Takara Bio, Japan). The resulting plasmids were digested with SmaI, and PCR-amplified genomic fragments containing the coding region and the 3′-region of *PATROL1* were inserted into the SmaI-digested vectors, to construct *gPATROL1:GUS-PATROL1* or *gPATROL1:EGFP-PATROL1*. Primers used for plasmid construction are listed in Table S1.

Transformation of *A. thaliana*.

Agrobacterium tumefaciens strain GV3101 was transformed with the appropriate construct and then used to transform *A. thaliana patrol1* mutants by the floral-dip method (54).

Co-IP analysis

Approximately 300 mg of 7-day-old *A. thaliana* roots expressing either GFP-PATROL1 (18) or GFP alone was ground in liquid nitrogen and homogenized in 900 μL of cold lysis buffer (50 mM Tris–HCl, pH 7.5, 150 mM NaCl, 1 mM EDTA, 1% Triton X-100, and a protease inhibitor cocktail). The homogenates were centrifuged at 15,000×g for 10 min at 4 °C. The supernatants were immunoprecipitated with a μMACS GFP Isolation Kit (Miltenyi Biotec, Japan), according to the manufacturer's instructions. The immunoprecipitates were separated by SDS-PAGE and immunoblotted with an anti-GFP antibody (sc-9996, 1:1,000 dilution; Santa Cruz Biotechnology, USA) or an anti-AHA2-cat polyclonal antibody (1:3,000 dilution; kindly provided by Dr. Toshinori Kinoshita (55)). Secondary antibodies—antimouse IgG, HRP-Linked Whole Ab Sheep (NA931, 1:10,000 dilution; GE Healthcare, USA), and antirabbit IgG, HRP-Linked Whole Ab Donkey (NA934, 1:10,000 dilution; GE Healthcare, USA)—were used to detect the primary antibodies on SuperSignal West Dura Extended Duration Substrate (34,076; Thermo Fisher Scientific, USA). A protein–protein BLAST search showed that the AHA2 antibody recognition sequence (55) shared high identity with those of all AHA isoforms (Table S2).

Histochemical analysis of GUS staining

Two-week-old *gPATROL1:GUS-PATROL1* plants were prefixed in ice-cold 90% (v/v) acetone for 15 min. The fixed samples were rinsed several times in sterile deionized water and incubated in staining buffer (100 mM sodium phosphate buffer [pH 7.0], 0.1% Triton-X-100, 5 mM potassium ferrocyanide, 5 mM potassium ferricyanide, 10 mM EDTA, 0.5 mg/mL 5-bromo-4-chloro-3-indolyl-β-D-glucuronic acid) for 12 h at 37 °C. Stained samples were rinsed several times with 70% ethanol and transferred to chloral hydrate clearing solution (chloral hydrate/water/glycerol = 8:1:3 [w/v/v]) for observation.

qRT-PCR

Short-term effects of osmotic stress were observed by pouring 50 mL 30% (w/v) PEG 6000 onto 19-day-old *A. thaliana* grown on 1/2 MS gellan gum medium. Total RNA from shoots and roots was extracted with an RNeasy Plant Mini Kit (QIAGEN, Germany) and treated with DNase (TURBO DNA-free Kit; Thermo Fisher Scientific, USA), and cDNA was synthesized using the High Capacity RNA-to-cDNA Kit (Thermo Fisher Scientific, USA). Power SYBR Green PCR Master Mix (Thermo Fisher Scientific, USA) was used for qRT-PCR, and the $2^{-\Delta\Delta CT}$ method was used to calculate expression levels relative to *ACTIN 2* as an internal standard. Relative expression levels of all *A. thaliana* DUF810 and AHA member genes in the shoots and roots of 14-day-old plants grown on 1/2 MS gellan gum medium were similarly determined. Sequences of primers used for qRT-PCR are listed in Table S1.

Confocal microscopic analysis

Confocal microscopic analysis of EGFP-PATROL1 was performed using a C2 confocal Microscope (Nikon, Japan). With excitation at 488 nm, EGFP fluorescence was measured at 500–550 nm. Images were processed in NIS-Elements (Nikon, Japan) and ImageJ/Fiji software (56).

Roots of 1-week-old *gPATROL1:EGFP-PATROL1* transgenic plants, grown on the vertically oriented 1/2 MS gellan gum medium, were mounted between two different-sized coverslips 24 × 60 mm and 24 × 45 mm, with a sheet of Parafilm as a spacer, and the gap was filled with liquid 1/2 MS medium (sucrose-free, pH 5.7). For osmotic stress treatments, seedlings were perfused with liquid 1/2 MS medium with or without 10% (w/v) PEG 8000 (P5413; Sigma-Aldrich, USA) and incubated under the microscope for 30 min. Root epidermal cells were imaged through an inverted confocal microscope (FV1000; Olympus, Japan) with an air objective UPLSAPO 40X (NA 0.95, WD 0.18). GFP was excited at 473 nm with a multiline argon laser. Confocal Z-stacked images were acquired at 1-μm intervals before and after treatment. Images were processed and analyzed in ImageJ/Fiji software.

Root growth assay

Photographs were taken 10 days after PEG treatment with a digital single-lens reflex camera. Root length and numbers were manually measured in the ImageJ/Fiji software (56).

Gas exchange and chlorophyll fluorescence measurements

We measured gas exchange and chlorophyll fluorescence of WT, *patrol1*, and *PATROL1*-OX plants grown under elevated [CO_2] (1,500 μmol mol^{-1}) using a portable gas exchange system (LI-6400XT; LI-COR Biosciences, USA). Following overnight dark adaptation, we measured the light response of the CO_2 assimilation rate (A), the quantum yield of PSII (Y(II)), and NPQ at ambient and elevated [CO_2] (400 and 1,500 μmol mol^{-1}) and measured post-tillumination induction of A, Y(II), NPQ, stomatal conductance (g_s), intercellular [CO_2](C_i), and intrinsic water use efficiency (iWUE) at elevated [CO_2] under PPFD of 500 μmol m^{-2} s^{-1}.

Following overnight dark adaptation, chlorophyll fluorescence was determined by a pulse-amplitude-modulated fluorometer (IMAG-MAX/L; Heinz Walz, Germany). Measurements were taken under actinic light intensity of growing light (GL, PPFD 100 μmol m^{-2} s^{-1}) or high light (HL, PPFD 500 μmol m^{-2} s^{-1}). The saturation pulse was applied at an intensity of 10 for 720 ms, with a measuring light intensity of 2, a frequency of 1 Hz, gain set to 2, and damping set to 2. Fluorescence was measured every 30 s after light irradiation, and we calculated the maximum quantum yield of PSII (Fv/Fm), Y(II), NPQ, quantum yield of regulated thermal dissipation in PSII (Y(NPQ)), that of nonregulated energy dissipation in PSII (Y(NO)), and fraction of open PSII reaction centers (qL) as described (25, 57).

Measurements of $\delta^{13}C$ discrimination

$\delta^{13}C$ of harvested shoots was determined with a CN analyzer (Vario Micro; Elementar Analyzensysteme, Germany) connected

to an isotopic ratio mass spectrometer (IsoPrime 100; Iso prime, United Kingdom). $\delta^{13}C$ values (‰) were calculated as described (58).

Determination of total carbon and nitrogen contents

Harvested shoots were oven-dried at 80 °C for 72 h to a constant weight and weighted. Samples were ground to a fine powder, and total C and N contents were determined by element analyzer (SUMIGRAPH NC-22F; Sumika Chemical Analysis Service, Japan).

Statistical analysis

All *n* values and statistical tests used are indicated in the figure legends. Data were analyzed by two-tailed t test or by one-way ANOVA with Dunnett's or Tukey's post hoc test at $P < 0.05$ in R v. 4.3.1 software (https://www.r-project.org/).

Acknowledgments

The authors thank Dr. Hashimoto-Sugimoto Mimi and Dr. Iba Koh (Kyusyu University) for providing the seeds, Dr. Toshinori Kinoshita (Nagoya University) for supplying the AHA2 antibody, Dr. Seo Mitsunori (University of the Ryukyus) for guidance on micrografting, and Dr. Taneda Haruhiko, Dr. Masaru Kono, and Dr. Qu Yuchen (The University of Tokyo) for their technical support with $\delta^{13}C$ discrimination measurements and for their valuable discussions. The authors extend their gratitude to all reviewers for their insightful comments and suggestions.

Supplementary Material

Supplementary material is available at *PNAS Nexus* online.

Fundings

This work was supported by Japan Society for the Promotion of Science (18KK0170, 21H02171, and 24H02277 to W.Y.) and Japan Science and Technology Agency (JPMJSP2108 to N.K.).

Author Contributions

N.K., K.S., H.K., I.T., and W.Y. contributed to the conceptualization of the study. N.K., K.S., H.K., and W.Y. were responsible for data curation. N.K., Y.Sh., Y.Sa., and W.Y. carried out formal analysis. N.K. and W.Y. acquired funding. N.K., K.S., H.K., Y.Sh., Y.Sa., K.N., and M.A. conducted the investigation. N.K., I.T., and W.Y. were responsible for methodology and administered the project. K.N. and M.A. provided resources. W.Y. supervised the study. N.K., Y.Sh., and Y.Sa. performed visualization. All authors contributed to writing the original draft, reviewing, and editing the manuscript.

Preprints

This manuscript was posted on a preprint: https://doi.org/10.1101/2024.11.04.621996.

Data Availability

All data are included in the manuscript and/or supporting information.

References

1 Rezaei EE, *et al.* 2023. Climate change impacts on crop yields. *Nat Rev Earth Environ*. 4:831–846.
2 Vadez V, *et al.* 2024. Crop traits and production under drought. *Nat Rev Earth Environ*. 5:211–225.
3 Plett DC, *et al.* 2020. The intersection of nitrogen nutrition and water use in plants: new paths toward improved crop productivity. *J Exp Bot*. 71:4452–4468.
4 Tardieu F, Simonneau T, Muller B. 2018. The physiological basis of drought tolerance in crop plants: a scenario-dependent probabilistic approach. *Annu Rev Plant Biol*. 69:733–759.
5 Moshelion M. 2020. The dichotomy of yield and drought resistance. *EMBO Rep*. 21:e51598.
6 Li S, *et al.* 2018. Modulating plant growth–metabolism coordination for sustainable agriculture. *Nature*. 560:595–600.
7 Zhang M, *et al.* 2021. Plasma membrane H^+-ATPase overexpression increases rice yield via simultaneous enhancement of nutrient uptake and photosynthesis. *Nat Commun*. 12:735.
8 Tanaka Y, Adachi S, Yamori W. 2019. Natural genetic variation of the photosynthetic induction response to fluctuating light environment. *Curr Opin Plant Biol*. 49:52–59.
9 Garcia A, *et al.* 2023. Enhancing crop yields through improvements in the efficiency of photosynthesis and respiration. *New Phytol*. 237:60–77.
10 Suralta RR, *et al.* 2018. Root plasticity for maintenance of productivity under abiotic stressed soil environments in rice: progress and prospects. *Field Crops Res*. 220:57–66.
11 Giehl RFH, von Wirén N. 2014. Root nutrient foraging. *Plant Physiol*. 166:509–517.
12 Li Y, Zeng H, Xu F, Yan F, Xu W. 2022. H^+-ATPases in plant growth and stress responses. *Annu Rev Plant Biol*. 73:495–521.
13 Zeng H, *et al.* 2024. Plasma membrane H^+-ATPases in mineral nutrition and crop improvement. *Trends Plant Sci*. 29:978–994.
14 Wang Y, *et al.* 2014. Overexpression of plasma membrane H^+-ATPase in guard cells promotes light-induced stomatal opening and enhances plant growth. *Proc Natl Acad Sci U S A*. 111:533–538.
15 Toh S, *et al.* 2021. Overexpression of plasma membrane H^+-ATPase in guard cells enhances light-induced stomatal opening, photosynthesis, and plant growth in hybrid aspen. *Front Plant Sci*. 12:766037.
16 Gévaudant F, *et al.* 2007. Expression of a constitutively activated plasma membrane H^+-ATPase alters plant development and increases salt tolerance. *Plant Physiol*. 144:1763–1776.
17 Merlot S, *et al.* 2007. Constitutive activation of a plasma membrane H^+-ATPase prevents abscisic acid-mediated stomatal closure. *EMBO J*. 26:3216–3226.
18 Hashimoto-Sugimoto M, *et al.* 2013. A Munc13-like protein in *Arabidopsis* mediates H^+-ATPase translocation that is essential for stomatal responses. *Nat Commun*. 4:2215.
19 Bhaskar BR, *et al.* 2024. Differential SNARE chaperoning by Munc13-1 and Munc18-1 dictates fusion pore fate at the release site. *Nat Commun*. 15:4132.
20 Ichita M, Higaki T. 2023. Intracellular trafficking regulation of plasma membrane H^+-ATPase and environmental response in plants. *Cytologia (Tokyo)*. 88:169–173.
21 Kimura H, Hashimoto-Sugimoto M, Iba K, Terashima I, Yamori W. 2020. Improved stomatal opening enhances photosynthetic rate and biomass production in fluctuating light. *J Exp Bot*. 71:2339–2350.
22 Notaguchi M, *et al.* 2024. The PATROL1 function in roots contributes to the increase in shoot biomass. *Planta*. 260:105.

23 Higaki T, Hashimoto-Sugimoto M, Akita K, Iba K, Hasezawa S. 2014. Dynamics and environmental responses of PATROL1 in arabidopsis subsidiary cells. *Plant Cell Physiol*. 55:773–780.

24 Hu C, Elias E, Nawrocki WJ, Croce R. 2023. Drought affects both photosystems in *Arabidopsis thaliana*. *New Phytol*. 240:663–675.

25 Kono M, Oguchi R, Terashima I. *Photoinhibition of PSI and PSII in nature and in the laboratory: ecological approaches*. Springer, Cham, 2022. p. 241–292.

26 Miyake C. 2010. Alternative electron flows (water–water cycle and cyclic electron flow around PSI) in photosynthesis: molecular mechanisms and physiological functions. *Plant Cell Physiol*. 51:1951–1963.

27 Rogers ED, Benfey PN. 2015. Regulation of plant root system architecture: implications for crop advancement. *Curr Opin Biotechnol*. 32:93–98.

28 Sato F, Iba K, Higaki T. 2021. Involvement of the membrane trafficking factor PATROL1 in the salinity stress tolerance of *Arabidopsis thaliana*. *Cytologia (Tokyo)*. 86:119–126.

29 Wang S, Ma C. 2022. Neuronal SNARE complex assembly guided by Munc18-1 and Munc13-1. *FEBS Open Bio*. 12:1939–1957.

30 Basu J, *et al.* 2005. A minimal domain responsible for Munc13 activity. *Nat Struct Mol Biol*. 12:1017–1018.

31 Stevens DR, *et al.* 2005. Identification of the minimal protein domain required for priming activity of Munc13-1. *Curr Biol*. 15: 2243–2248.

32 Xia L, Marquès-Bueno MM, Bruce CG, Karnik R. 2019. Unusual roles of secretory SNARE SYP132 in plasma membrane H +-ATPase traffic and vegetative plant growth. *Plant Physiol*. 180: 837–858.

33 Xue Y, Yang Y, Yang Z, Wang X, Guo Y. 2018. VAMP711 is required for abscisic acid-mediated inhibition of plasma membrane H^+-ATPase activity. *Plant Physiol*. 178:1332–1343.

34 Xue Y, Zhao S, Yang Z, Guo Y, Yang Y. 2019. Regulation of plasma membrane H^+-ATPase activity by the members of the V-SNARE VAMP7C family in *arabidopsis thaliana*. *Plant Signal Behav*. 14: 762–778.

35 Baena G, Xia L, Waghmare S, Karnik R. 2022. SNARE SYP132 mediates divergent traffic of plasma membrane H^+-ATPase AHA1 and antimicrobial PR1 during bacterial pathogenesis. *Plant Physiol*. 189:1639–1661.

36 Baena G, *et al.* 2024. Arabidopsis SNARE SYP132 impacts on PIP2;1 trafficking and function in salinity stress. *Plant J*. 118:1036–1053.

37 Fujiwara M, *et al.* 2014. Interactomics of Qa-SNARE in *Arabidopsis thaliana*. *Plant Cell Physiol*. 55:781–789.

38 Haruta M, Tan LX, Bushey DB, Swanson SJ, Sussman MR. 2018. Environmental and genetic factors regulating localization of the plant plasma membrane H^+-ATPase. *Plant Physiol*. 176: 364–377.

39 Młodzińska E, Kłobus G, Christensen MD, Fuglsang AT. 2015. The plasma membrane H^+-ATPase AHA2 contributes to the root architecture in response to different nitrogen supply. *Physiol Plant*. 154:270–282.

40 Pacifici E, Di Mambro R, Dello Ioio R, Costantino P, Sabatini S. 2018. Acidic cell elongation drives cell differentiation in the *Arabidopsis* root. *EMBO J*. 37:e99134.

41 Młodzinska-Michta E. 2022. Root system responses to phosphate nutrition involve plasma membrane H^+-ATPases in *Arabidopsis thaliana*. *Acta Physiol Plant*. 44:1–12.

42 Xu W, *et al.* 2013. Abscisic acid accumulation modulates auxin transport in the root tip to enhance proton secretion for maintaining root growth under moderate water stress. *New Phytol*. 197:139–150.

43 Li L, *et al.* 2021. Cell surface and intracellular auxin signalling for H^+ fluxes in root growth. *Nature*. 599:273–277.

44 Meier M, *et al.* 2020. Auxin-mediated root branching is determined by the form of available nitrogen. *Nat Plants*. 6:1136–1145.

45 Miao R, *et al.* 2018. Comparative analysis of Arabidopsis ecotypes reveals a role for brassinosteroids in root hydrotropism. *Plant Physiol*. 176:2720–2736.

46 Yuan W, *et al.* 2018. BR-INSENSITIVE1 regulates hydrotropic response by interacting with plasma membrane H^+-ATPases in Arabidopsis. *Plant Signal Behav*. 13:e1486147.

47 Monden K, *et al.* 2022. Root-specific activation of plasma membrane H^+-ATPase 1 enhances plant growth and shoot accumulation of nutrient elements under nutrient-poor conditions in *Arabidopsis thaliana*. *Biochem Biophys Res Commun*. 621:39–45.

48 Ding M, *et al.* 2022. Overexpression of a plasma membrane H^+-ATPase gene OSA1 stimulates the uptake of primary macronutrients in rice roots. *Int J Mol Sci*. 23:13904.

49 Kinoshita SN, Suzuki T, Kiba T, Sakakibara H, Kinoshita T. 2023. Photosynthetic-product–dependent activation of plasma membrane H^+-ATPase and nitrate uptake in *Arabidopsis* leaves. *Plant Cell Physiol*. 64:191–203.

50 Zhu X, Li S, Pan S, Xin X, Gu Y. 2018. CSI1, PATROL1, and exocyst complex cooperate in delivery of cellulose synthase complexes to the plasma membrane. *Proc Natl Acad Sci U S A*. 115: E3578–E3587.

51 Zhang SS, *et al.* 2016. Cellulose synthesis genes *CESA6* and *CSI1* are important for salt stress tolerance *in Arabidopsis*. *J Integr Plant Biol*. 58:623–626.

52 Turnbull CGN, Booker JP, Leyser HMO. 2002. Micrografting techniques for testing long-distance signalling in *Arabidopsis*. *Plant J*. 32:255–262.

53 Tsutsui H, *et al.* 2020. Micrografting device for testing systemic signaling in Arabidopsis. *Plant J*. 103:918–929.

54 Clough SJ, Bent AF. 1998. Floral dip: a simplified method for Agrobacterium-mediated transformation of *Arabidopsis thaliana*. *Plant J*. 16:735–743.

55 Hayashi Y, *et al.* 2010. Biochemical characterization of in vitro phosphorylation and dephosphorylation of the plasma membrane H^+-ATPase. *Plant Cell Physiol*. 51:1186–1196.

56 Schindelin J, *et al.* 2012. Fiji: an open-source platform for biological-image analysis. *Nat Methods*. 9:676–682.

57 Kramer DM, Johnson G, Kiirats O, Edwards GE. 2004. New fluorescence parameters for the determination of QA redox state and excitation energy fluxes. *Photosynth Res*. 79:209–218.

58 Sugiura D, Terashima I, Evans JR. 2020. A decrease in mesophyll conductance by cell-wall thickening contributes to photosynthetic downregulation. *Plant Physiol*. 183:1600–1611.